ADVANCED FUNCTIONAL MATERIALS
www.afm-journal.de

Highly Conductive Few-Layer Graphene/Al_2O_3 Nanocomposites with Tunable Charge Carrier Type

*Yuchi Fan, Wan Jiang, and Akira Kawasaki**

An ex situ strategy for fabrication of graphene oxide (GO)/metal oxide hybrids without assistance of surfactant is introduced. Guided by this strategy, GO/Al_2O_3 hybrids are fabricated by two kinds of titration methods in which GO and Al_2O_3 colloids are utilized as titrant for hybrids of low and high GO content respectively. After sintered by spark plasma sintering, few-layer graphene (FG)/Al_2O_3 nanocomposites are obtained and GO is well reduced to FG simultaneously. A percolation threshold as low as 0.38 vol.% is achieved and the electrical conductivity surpasses 10^3 Sm^{-1} when FG content is only 2.35 vol.% in FG/Al_2O_3 composite, revealing the homogeneous dispersion and high quality of as-prepared FG. Furthermore, it is found that the charge carrier type changes from p- to n-type as graphene content becomes higher. It is deduced that this conversion is related to the doping effect induced by Al_2O_3 matrix and is thickness-dependent with respect to FG.

1. Introduction

Graphene/metal oxide hybrids and composites have received great attention due to the synergetic effects provided by the combination of metal oxides and graphene, which can prominently improve the performance comparing with individual metal oxides. These novel composites have broad applications in the field of drug delivery,[1] lithium ion battery,[2] super capacitors and transparent conductors,[3] etc. However, the main obstacle lying in the preparation of graphene/metal oxide composits is to disperse graphene homogeneously throughout the oxides, since the agglomeration would deteriorate the electrical, optical and magnetic properties of the composites. To solve this problem, considerable efforts have been made but challenges still remain. On one hand, most of current methods to prepare graphene/metal oxide composites are based on an *in situ* growth strategy,[4] as a result it is very difficult to control the quality and morphology of metal oxides at will because of the presence of graphene. In this sense it would be more desirable that an *ex situ* method could be adopted. Specifically, graphene (or graphene oxide (GO)) and metal oxides are prepared separately at first and then combined together through certain ways. Thereby the preparation of metal oxide could be optimized easily and many commercially available oxide powders with high quality (such as α-Al_2O_3 and TiO_2) can be exploited directly for optimizing the performance of composites. On the other hand, many of those methods include the usage of surfactants which could either assist the dispersion of metal oxide or facilitate the formation of special structure.[2b,5] However, the residue of surfactants will probably harm the performance of composites.[6] Moreover, removing these surfactants often requires multiple washings or harsh conditions such as heating at high temperature, which is not feasible for many metal oxides.

Although many graphene/metal oxide hybrids have been reported, very few works have been carried out to further densify those hybrids to obtain composites and study the properties in a filler/matrix system. In our previous work, fully dense graphene nanosheet/Al_2O_3 composites were fabricated by ball milling and spark plasma sintering (SPS) for the first time.[7] It has been proved that the electrical properties of graphene based composites were far better than those of carbon nanotube based composites. Albeit the dispersion of graphene in the matrix is quite well, the percolation threshold is still higher than that of corresponding carbon nanotube based composite since the average thickness of graphene flakes are not thin enough to be qualified as graphene according to the classic definition.[8] Like the agglomeration of carbon nanotubes, thick graphite flakes are also harmful especially for the mechanical properties of composites.[9]

In this study, commercially obtained α-Al_2O_3 is taken as an example to elucidate a strategy of utilizing electrostatic interaction for the preparation of GO/metal oxide hybrids without assistance of surfactant. Two kinds of titration methods were conducted to prepare hybrids with low and high GO contents, respectively. Scanning electron microscopy (SEM) and transmittance electron microscopy (TEM) images show homogeneous dispersion of GO among Al_2O_3 particles. After densified by SPS, the morphology and thickness of few-layer graphene (FG) in composite were confirmed by TEM and high resolution TEM (HRTEM). The reduction level and quality of FG in composite were characterized by XPS and Raman spectra. Electrical

Dr. Y. Fan, Prof. Dr. A. Kawasaki
Department of Materials Processing
Graduate School of Engineering
Tohoku University
Sendai 980-8579 Japan
E-mail: kawasaki@material.tohoku.ac.jp
Prof. Dr. W. Jiang
State Key Laboratory for Modification of Chemical Fibers and Polymer Materials
Donghua University
Shanghai 201620, China

DOI: 10.1002/adfm.201200632

conductivity measurement demonstrated that extremely low percolation threshold has been achieved in this FG/Al_2O_3 composite and high electrical conductivity composite can be obtained at very low graphene content. Hall coefficient measurement revealed that the carrier type is p-type when graphene content is low but changes to n-type when graphene content becomes high, which has been explained neatly.

2. Results and Discussion

2.1. Preparation of GO/Al_2O_3 Hybrids

It is well known that water can be chemisorbed on oxides though a hydrogen bond or it may undergo dissociation. In the latter case, surface hydroxyl groups are formed.[10] Therefore for metal oxide particles, in most cases H^+ and OH^- are preferentially adsorbed on the particles and determine the electrical potential of the particle surface so that the particles can be positively or negatively charged by simply adjusting pH:

$$M - OH_2^+ \Longleftrightarrow M - OH + H^+ \quad (1)$$

$$M - OH \Longleftrightarrow M - O^- + H^+ \quad (2)$$

On the behalf of GO, although the differences in starting materials and oxidation protocol lead to an ambiguous structure of GO in some extent, it is generally accepted that the dominant structural features present on the surface of GO are tertiary alcohols, ethers (mainly in the form of epoxides) and carboxyl groups at the edges.[11] Thanks to the abundance of these kind of groups, GO exhibits a significant zeta potential even under highly acidic conditions, which is sufficient for the exfoliation and dispersion of GO in water, as seen in **Figure 1**. Moreover, the surface charge of GO remains a value smaller than –40 mV in a wide range (Figure 1, indicated by the arrow with dot line) which leaves large flexibility for adjusting pH until the surface of metal oxide becomes positive charged. This is very important because most of metal oxides have been reported as a component of graphene hybrids (P25, magnetite, hematite, β-MnO_2, ZnO, SnO_2, etc) have a "zero-point charge" (z.p.c.) larger than 4,[12] which means for any of these metal oxides there is a pH value below which GO and the metal oxide possess opposite surface charge. Therefore when the two species are mixed together they will assemble spontaneously under the mutual electrostatic interactions. Besides, the agglomeration of GO could be prevented by a steric effect stemming from the existence of metal oxide particles between GO flakes.

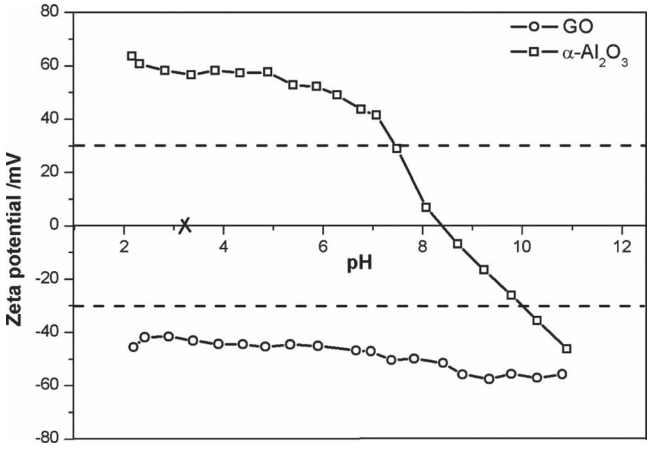

Figure 1. Zeta potential of GO and α-Al_2O_3 as a function of pH in aqueous dispersions; the cross denotes the pH adopted in this work.

In this work commercially obtained α-Al_2O_3 powder with high quality was chosen to illustrate our strategy. As shown in Figure 1, the z.p.c of Al_2O_3 is around 9 so that theoretically any pH environment below 9 will lead to an effective attraction between GO and Al_2O_3 particles. Since a zeta potential of larger than 30 mV is generally considered to represent sufficient mutual repulsion ensuring a stable dispersion,[13] any pH value below 7.5 would be suitable for the fabrication of GO/Al_2O_3 hybrids. Considering the as-prepared GO colloid had a pH of 3.3, we chose this value for convenience. In practice, the steric effect could be realized in two kinds of titration methods. When GO colloid was added into Al_2O_3 colloid drop by drop (denoted by GO^MO here and after), very small amount of GO (1.23 wt.% in hybrid) was high enough to precipitate all the Al_2O_3 particles and a transparent supernatant was left. However, when the GO content was over 1.92 wt.% the supernatant was not transparent anymore. Increasing the amount of GO could change the color of supernatant gradually until it reached that of pristine GO colloid, revealing that a limit had come. In addition, GO can be hardly observed by SEM or by TEM at low magnification in the hybrids prepared by GO^MO method (**Figure 2**a, b and c). It only can be observed at the edge of powders when the magnification of TEM is high enough, from which we can see ultrathin GO wrapped on the surface of Al_2O_3 particles closely (Figure 2d). In contrast, when small amount of Al_2O_3 colloid was added into the GO colloid in titration way (denoted by MO^GO here and after), the relative amount of GO could be very high. In our work hybrids with GO content up to 11.5wt.% have been prepared by MO^GO method. SEM images show that Al_2O_3 particles were wrapped by GO to form small packages (**Figure 3**a and b) and many particles were even separated from each other by GO (Figure 3b). This GO-encapsulated structure can be seen more clearly in TEM images (Figure 3d). In addition, although it is shown that the dispersion of GO flakes among Al_2O_3 particles was still homogeneous at such high content, the average thickness of GO layers mildly increased because of restacking (Figure 3c and d).

The reason why the two types of titration methods have such different ability of mixing can be demonstrated as follows. In the GO^MO method, each piece of added GO is surrounded by excessive metal oxide particles which will instantly adhere to GO as many as possible. On one hand, each piece of GO will reach its maximum ability of carrying metal oxide particles as soon as added to the colloid. On the other hand, the surface potential of carried metal oxide particles are shielded by GO in certain extent. GO has the ability to lock these particles but not necessarily enwraps them completely. Hence most of metal oxide particles are only partially shielded by GO at the beginning and they still have the ability to accept other GO on the exposed surfaces (**Figure 4**a). When more and

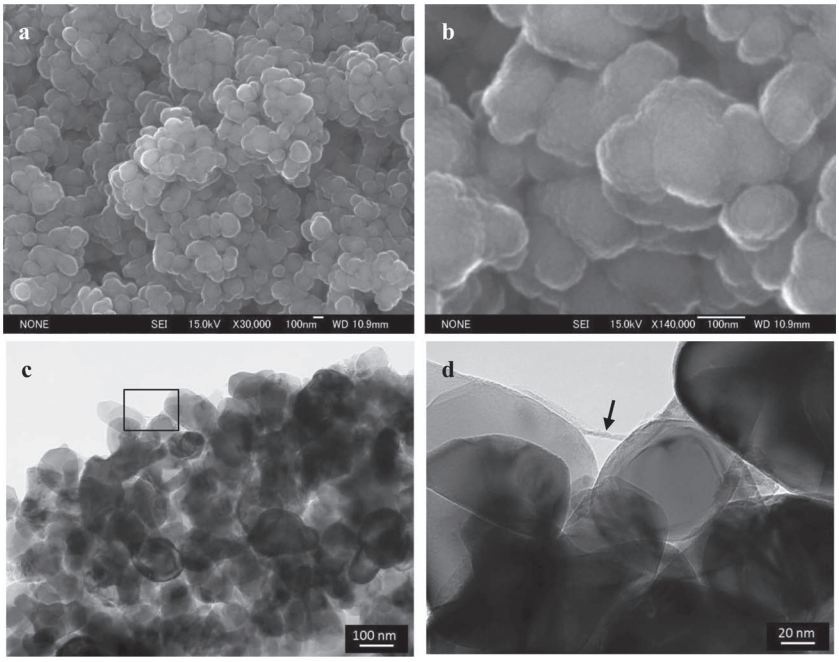

Figure 2. Morphology of GO/Al_2O_3 hybrid with GO content of 1.92 wt.% prepared by GO^MO method. (a), (b) are SEM images of lower and higher magnification, respectively; (c) is TEM image and (d) is a magnified part of the box in (c); the black arrow in (d) indicates the GO flake covering on Al_2O_3 particles.

more GO are added to colloid, the exposed surfaces decrease rapidly and finally all the particles are fully wrapped, as illustrated by Figure 4b. Any newly added GO will be repelled by these existing GO/metal oxide hybrid unit and stay in the supernatant since all the components in the solution are ether negatively charged or shielded by negatively charged GO at this moment. If we denote the content of GO that can barely makes the MO particles deposited as χ_0 and the limit of using GO^MO method as χ_m, the range $\Delta\chi = \chi_m - \chi_0$ is very small because of the extremely high surface area (2630 m^2g^{-1}, calculated). In the MO^GO method, GO pieces are hardly saturated because of the relatively small amount of MO particles compared with GO. In an ideal situation each piece of GO will bear the added particles equally, so that no extra particle will exist until χ_0. However, empirically GO content could never reach χ_0 by MO^GO method before extra particles started to appear. This is mainly because GO will precipitate prematurely before its maximum ability of carrying MO particles comes, which has been confirmed by monitoring the change of zeta potential (Supporting Information, S1). Hence the MO^GO method is suitable for preparing GO/metal oxide hybrids with high content of GO, while GO^MO method is more convenient for lower GO content.

2.2. Microstructure of FG/Al_2O_3 Composites

The properties of composites depend strongly on how well the filler materials are dispersed, which is the reason why many composites researches relating to carbon nanotubes have focused on finding better methods for dispersing nanotubes into matrix. Since graphene and GO are two-dimensional materials, entangled bundles usually found in carbon nanotubes are no longer an issue. However, aggregation is still possible and should be avoided. In our method, benefiting from the good dispersion of GO in hybrids, aggregation of FG did not happen after sintering, which has been confirmed by TEM (**Figure 5**). It clearly shows that FG flakes were located between the boundaries of Al_2O_3 particles and they are readily to be found even if the content of graphene is very low (Figure 5a). The representative thickness of FG is round 1.2 nm which contains 4 layers of graphene (Figure 5b). According to our observation, layers of thickness larger than 3 nm have never been found in this particular sample, which indicates the success of our strategy in homogeneous dispersion of graphene in matrix. However, the overlapped graphene flakes of larger thickness (~5 nm) can be observed in the composite with higher graphene content (Figure 5c,d). This kind of junction is

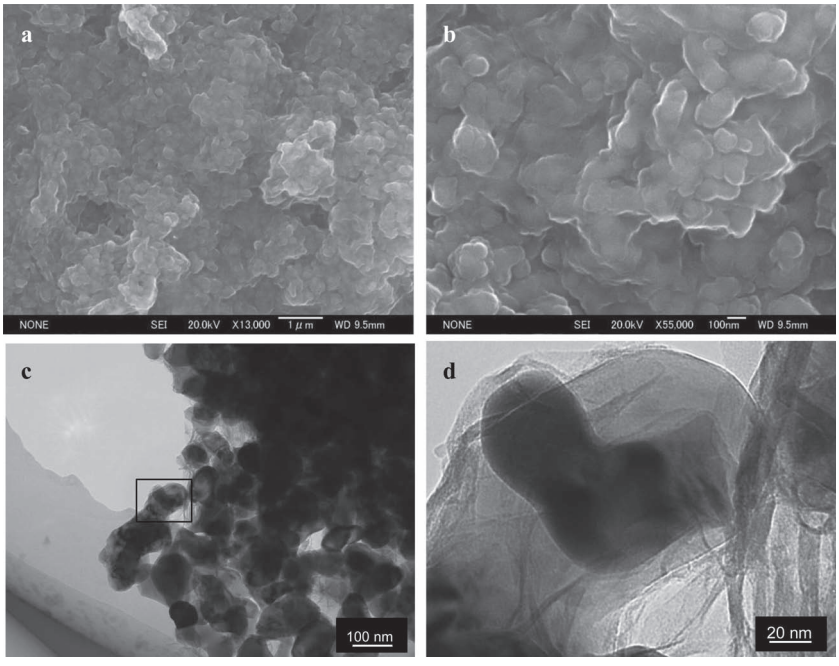

Figure 3. Morphology of GO/Al_2O_3 hybrid with GO content of 11.5wt.% prepared by MO^GO method. (a), (b) are SEM images of lower and higher magnification, respectively; (c) is TEM image and (d) is a magnified part of the box in (c) which shows a single Al_2O_3 particle wrapped by GO flake.

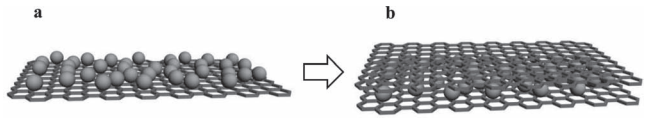

Figure 4. Metal oxide particles partially shielded (a) and completely shielded by GO (b) in GO^MO method.

necessary for the connection of neighboring flakes to form an conductive network, but the average thickness of graphene will inevitably increase at the same time.

A very interesting phenomenon found by TEM is the morphology of FG after ion beam milling. It is found that residual parts of FG always exist outside the polishing surface, as indicated in Figure 5a. The HRTEM image shows that the residual part is parallel to the polishing surface and contains very rough edge (Figure 5b) which looks like to be torn up by the argon ion beam. The phenomenon can be understood by the extremely thin feature of as-prepared FG. Firstly, because of the complexity of distribution and type of defect in graphene, the fracture surface is not smooth and some tiny parts with relatively high strength will remain and be exposed from the matrix when the covered Al_2O_3 are removed by ion beam. Secondly, these residual parts will attach to the polished surface because FG is prone to deform. Since the thickness of protruding parts is very small (~1 nm) and they are nearly parallel to the direction of ion beam, these parts have large possibility to survive from ion beam milling. However, if there are too many layers of graphene in one flake, it will become difficult to deform so that any protruding part will be "cut" smoothly, which is the reason why similar phenomenon has never been observed in multi-walled carbon nanotube/Al_2O_3 composite and graphene nanosheet/Al_2O_3 composite in which graphene nanosheet can be as thick as 10 nm.[7,14]

2.3. Reduction of GO and Quality of As-Prepared FG

The reduction process is necessary for GO because it's an electrically insulating material owning to the disrupted sp^2 bonding network. Among the reduction methods, thermal treatment has been found to be one of the most effective.[15] Since SPS itself is a high temperature process with low atmosphere pressure (1300 °C and P < 6 Pa in this work), there is no need of additional reduction procedure. However, it has to be noticed that the thermal stability of GO is very weak. Thermal decomposition of GO begins at very low temperature (~177 °C),[16] with release of H_2O, CO and CO_2 in gas phase. In addition, around 70% mass loss has been observed when the temperature reached as high as 700 °C in thermal analysis.[15] Therefore the mass loss caused by high temperature sintering has to be measured in order to estimate the thermal stability of GO at sintering temperature. During thermo-gravimetric analysis (TGA), ~60% mass was lost before 300 °C and the total mass remained only 13.07% after temperature rose to 1300 °C (**Figure 6**a). However, experiment indicated that the real remained mass of GO after sintering was as much as 35% (see Experimental Section), probably benefiting from the fast heating rate and low atmosphere pressure during SPS. The reduction of GO is confirmed by comparing high resolution x-ray photoelectron spectroscopy (XPS) from the carbon region of GO and FG in sintered composite. Three most prominent components are assigned to the C 1s envelope, namely the sp^2 peak centered at 284.6 eV, C-O peak at 286.6 eV and C = O peak at 288.5 eV. Upon heating under SPS sintering, the C 1s spectrum exhibits a transformation from a double peak at room temperature to a single sharp peak after sintering, which is indicative of restored sp^2 bonding. In addition, it is illustrated that in the composite sample only a very weak C-O peak can be deconvoluted from C 1s envelope whereas the C = O component is barely differentiated, revealing that the amount of remaining oxygen is very low.

The quality of FG in composites with different content was further investigated by Raman spectroscopy and compared with GO and raw graphite (**Figure 7**). The main

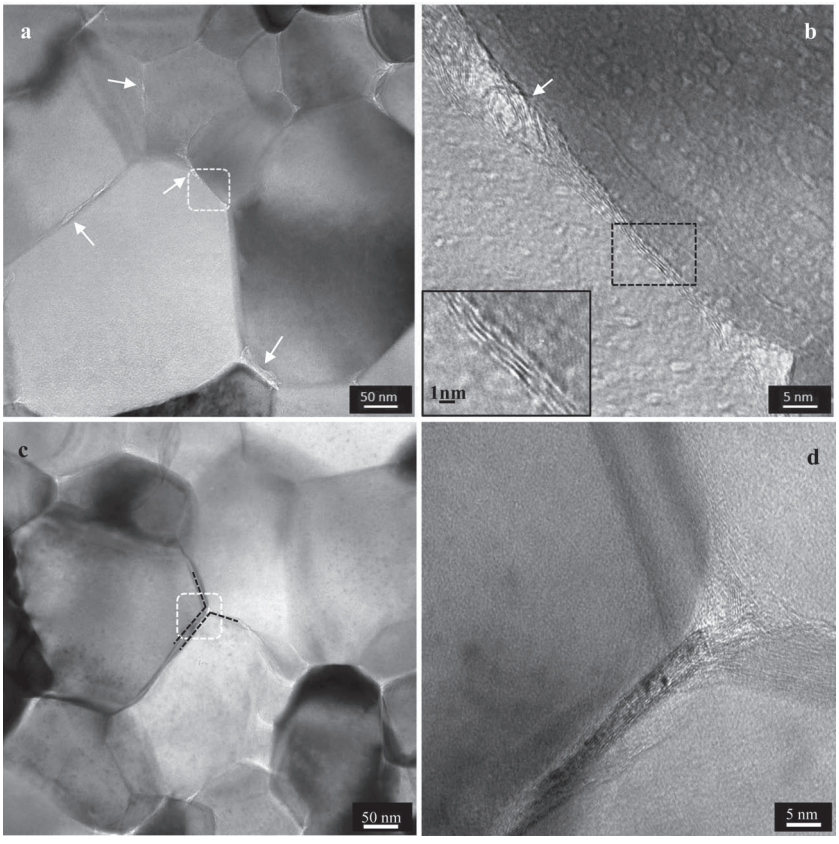

Figure 5. TEM and HRTEM images of FG/Al_2O_3 composites with graphene content of 0.66 vol.% ((a) and (b)) and 1.56 vol.% ((c) and (d)); (b) and (d) are HRTEM images of the white boxes in (a) and (c), respectively. The arrows in (a) and (b) indicate the residual FG outside the polishing surface and the dash lines in (c) indicate the overlapped FG.

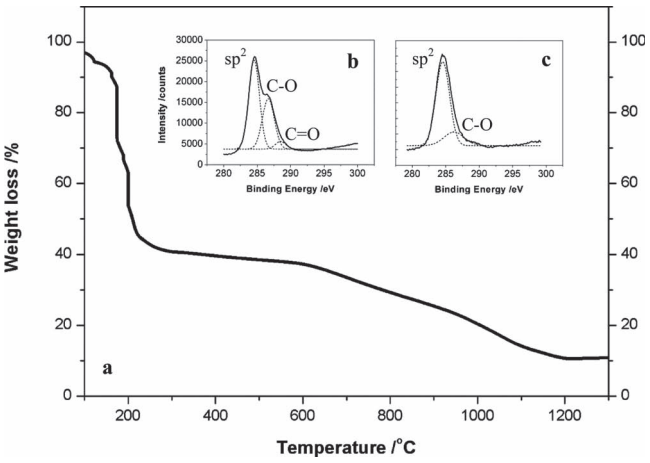

Figure 6. (a) The weight loss of GO powders from 100 to 1300 °C measured by TGA; it is assumed that the loss before 100 °C is ascribed to the evaporation of water and the weight loss is calculated from 100 °C. (b) and (c) are high resolution C 1s XPS spectra of GO and FG after sintering at 1300 °C, respectively.

features in the Raman spectra of sp^2 carbon materials are the G and D bands that lie at around 1580 and 1350 cm^{-1}, respectively. Both the G and D bands arise from vibrations of sp^2-hybridized carbon atoms and can be observed in GO and graphene in composites. On the contrary, in the SP-1 graphite the D band is too weak to be identified with respect to the G band, revealing the good quality of raw material. It is shown that G band shifts to higher frequency (~13 cm^{-1}) for GO and FG in composites compared with graphite, which is usually observed in oxidized graphene.[17] The ratio between the intensity of D and G bands has been widely used as an indicator of amount of disorders. In this work, it is observed that GO has a lower I_D/I_G compared to FG in composite, but the greatly broadening and overlapping G and D bands indicate GO contained higher amount of defects (Figure 7). In fact, I_D/I_G does not always increase monotonically with increasing defects in sp^2 carbon materials. It has been found that I_D/I_G will decrease

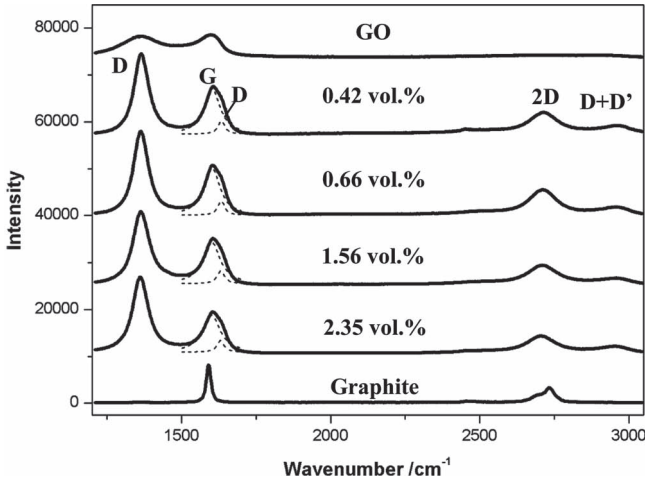

Figure 7. Raman spectra of GO, graphite and composites with graphene content of 0.42, 0.66, 1.56 and 2.35 vol.%.

with increasing amount of defects when graphene turns from nanocrystalline to amorphous, which can be understood through a competing mechanism proposed by Jorio et al.[18] It is very likely that chemically oxidized graphene follows the similar evolution relationship.

Instead of I_D/I_G, the separation of D′ from G band can be set as a criterion to further estimate the extent of reduction. Defects result in the appearance of D and D′ bands, but with increasing amount of defects D' will become stronger while shift to lower frequency and finally merge with G band.[18,19] Thus it is reasonable to conclude that the reversal process denotes the decreasing of defects. As shown in Figure 7, D′ band cannot be distinguished in GO, but in the composites its existence can be identified, indicating higher reduction level caused by high temperature sintering. The information contained in 2D band appearing around 2680 cm^{-1} can be set as another criterion. Although the shape of 2D band is generally used for quantifying the number of graphene layers, the identification is well established only for graphene that have AB bernal stacking.[20] Since most of the observed FG in the composites have 3 layers, the single lorentzian shape of G' band (Figure 7) suggests that the stacking of graphene was more like turbostratic after sintering. Rather than the shape of 2D band, it was found that the 2D to D+D′ intensity ratios ($I_{2D}/I_{D+D'}$) provide a better correlation with the reduction of graphene, because 2D band is sensitive to the aromatic carbon structure whereas the combination mode of D+D′ is lattice disorder induced band for crystalline graphitic materials.[21] This is consistent with our observation that 2D band of FG reappeared with increased $I_{2D}/I_{D+D'}$ in FG/Al_2O_3 composites. Besides, it is also can be seen that there is no noticeable difference of FG quality in composites with varying graphene content. To sum up, albeit certain amount of structural disorders were left in the graphene plane, a high level of reduction and graphitization has been achieved in as-prepared FG via SPS.

2.4. Electrical Properties of FG/Al_2O_3 Composites

For FG/Al_2O_3 composites, the filler volume fraction was calculated after considering the weight loss of GO during SPS (see Experimental Section). The electrical conductivity as a function of graphene volume fraction at room temperature is fitted by using the power law (**Figure 8**a):

$$\sigma_c = f[(\varphi - \varphi_c)/(1-\varphi_c)]^t \quad (3)$$

where σ_f is the conductivity of the filler, φ is the filler volume fraction, φ_c is the percolation threshold volume fraction and t is the universal critical exponent. The percolation threshold of FG/Al_2O_3 composite is only 0.38 vol.%, which is slightly higher than the prediction value of geometric percolation threshold (~0.13 vol.%) in the composite whose disk-shaped filler has an aspect ratio of 1000.[22] Interestingly, the percolation threshold is even lower than the best value obtained in carbon nanotube/metal oxide composites (0.64 vol.%),[23] whereas prolates (rod-like) are supposed to percolate at one-half the volume fraction of oblates (disk-like) according to the percolation theory.[22] The lower percolating value of FG/Al_2O_3 composite can be ascribed to a better dispersion of graphene

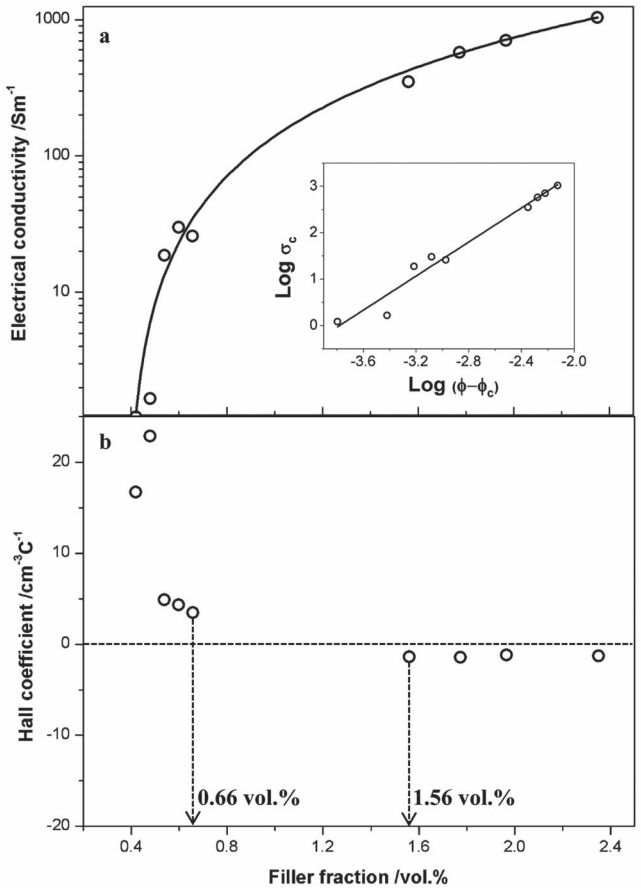

Figure 8. (a) Electrical conductivity of FG/Al_2O_3 composites (σ_c) as a function of filler volume fraction (φ), inset: log σ_c plotted against log($\varphi - \varphi_c$), where φ_c is the percolation threshold; (b) Hall coefficient (R_H) plotted against filler volume fraction (φ).

in the matrix and better contact between conductive nanoparticles.[7] Above percolation threshold, the electrical conductivity of FG/Al_2O_3 composite sharply increased with the graphene volume fraction, especially at low loading region. The electrical conductivity of FG/Al_2O_3 composite is more than 1 Sm^{-1} at only 0.42 vol.% and reaches 30 Sm^{-1} at only 0.6 vol.%. By increasing the graphene content to 2.35 vol.%, a conductivity of 1038.15 Sm^{-1} is achieved. Noticing that the conductive phase content should be as high as 5.7 vol.% in carbon nanotube/Al_2O_3 composite to reach the same level of conductivity,[24] this result shows the unparalleled advantage of graphene as reinforcing phase in composites compared with other carbon materials. In addition, it also proves the success of our method in homogeneous dispersion of FG and high level of reduction from GO. The electrical conductivity of as-prepared FG can be estimated by the linear fitting to the log-log plot of conductivity versus ($\varphi - \varphi_c$), which resulted in $t = 1.84 \pm 0.13$ and $\sigma_f \cong 9.67 \times 10^5$ Sm^{-1}. The calculated electrical conductivity is 35% higher than GO film annealed at 1100 °C,[15] benefitting from a higher temperature adopted in sintering process. However, the value was still lower than the intrinsic value of perfect graphene,[25] reflecting the significant influence of defects and ceramic environment.

To further explore the electrical properties of as-prepared composites, hall coefficient (R_H) of FG/Al_2O_3 composites (GO) with different graphene content was measured. Figure 8b shows that the absolute value of R_H decreased with increasing graphene content. Since increasing graphene content resulted in increasing charge density, this tendency reveals R_H obeyed the usual relation of $|R_H| \propto 1/ne$, where n is the charge density and e is the electron charge. However, it is striking to observe that hall coefficient reversed its sign from positive to negative after the graphene content became high, revealing the conversion of major charge carrier. We further confirmed this conversion by measuring the thermopower of composites. It is found that the Seebeck coefficient was positive in the composite with low graphene content, but changed to negative in the composite with high graphene content (supporting information, S2). This phenomenon is very unique that has never been observed in other composites. Usually the carrier type of composite is determined by the conductive filler and the intrinsic characteristics like carrier type do not depend on the filler material's quantity. In the case of graphene based composites, however, one thing that inevitably changes after filler content becoming high is the average thickness of FG flakes. When more and more graphene layers are dispersed in matrix, the opportunity of overlapping between different FG flakes will increase and sometimes the restacking cannot be avoided as well, which results in the rise of electrical conductivity and slightly increases the thickness of FG. Hence we deduce the conversion of carrier type is closely related to the increasing thickness of FG and can be interpreted as follows.

Firstly, the intrinsic carrier type of thermally reduced GO should be electron. It has been reported that the chemically reduced and annealed GO films (composed of 3–5 layers graphene) exhibit graphite-like semi-metals characteristics and the electron mobility is generally higher than the hole mobility in vacuum.[26] Thereby it can be inferred that the intrinsic carrier type of as-prepared graphene is more resembling to that of few layers graphene, since the C 1s peak of XPS spectra show that the reduction level of graphene in this work is better than the reported graphene film. Secondly, the positive Hall coefficient presumably arises from the doping induced by matrix. The influence of substrate to properties of graphene has been noticed since the discovery of graphene. It is found that when the interaction between graphene and substrate is weak, such as the situation that micromechanical cleaved graphene on different substrates, the influence of substrates is negligible.[27] However, when there is a strong interaction between graphene and substrate SiC substrate has no graphitic electronic properties and acts as a buffer layer that causes the subsequent graphene layer performs like isolated but doped graphene.[28] In FG/Al_2O_3 composite, the interaction between FG and matrix is strong because of the residual stress that stems from the difference of contraction after cooling. Graphene has a negative in-plane coefficient of linear thermal expansion from room temperature to 2000 K,[22,29] while Al_2O_3 has a positive one, which means during the cooling procedure graphene has a trend of expansion but the matrix will contract. As a result, great pressure will be generated and lead to very firm contact between FG and matrix. In addition, when exposed to environment of low oxygen partial pressure at high temperature,

oxygen vacancies $\left([V_o''] \propto (p_{o_2})^{-1/6}\right)$ and aluminum interstitials $\left([Al_i'''] \propto (p_{o_2})^{-3/16}\right)$ are promoted as main point defects.[30] These positively charged point defects act as electron acceptor to make graphene hole doped. Thus it can be inferred that the doping level depends on the concentration of oxygen vacancy and aluminum interstitials on the grain surface, but quantitative investigation will not be given here. Although only the outermost layers are doped by matrix, the inner layers also can be affected through charge transfer between layers. Therefore the Hall coefficient remains positive when most of flakes contain a few graphene layers, such as the situation in the composite with graphene content of 0.66 vol.% (Figure 5a and b). Finally, the Hall coefficient changes to negative when the graphene layers become thick. The electrical conductivity of composite can be enhanced by filler material in two ways. One is through establishing new conductive path in the matrix and the other is through increasing the cross area of formed path, which is the thickness of FG flakes in the case of graphene based composite. Because of the preparing strategy adopted in this study, the dispersion of FG in the matrix is homogeneous so that the former way is dominant when graphene content is low. Since new interfaces between FG and matrix continue forming in this procedure, the composites persist to be p-type. After graphene content becomes high, the conductivity will mainly increase through the second mechanism, such as the situation in the composite with graphene content of 1.56 vol.% (Figure 5c and d). Since the total amount of hole-type carrier keeps unchanged statistically, the doping level will decrease with increasing graphene content and eventually the composite will perform as n-type.

3. Conclusions

An *ex situ* strategy is introduced to prepare GO/metal oxide hybrids without assistance of surfactant. By controlling the electrostatic interaction between GO and metal oxide particles, the corresponding hybrid material with homogenous dispersion of GO can be fabricated. As an example, GO/Al_2O_3 hybrids has been obtained with GO composition in a range from 1.23 to 1.92wt.% and from 2.88 to 11.5 wt.% by using two kinds of titration methods respectively. For FG/Al_2O_3 composites, it is found by XPS and Raman spectra that the SPS treated FG flakes possess very high quality. Oweing to the homogenous dispersion of high-quality FG in matrix, the percolation threshold of FG/Al_2O_3 composite is as low as 0.38 vol.% and the electrical conductivity can reach 10^3 Sm^{-1} when graphene content is only 2.35 vol.%. More interestingly, the charge carrier type is p-type when graphene content is low and changes to n-type when graphene content increases to high level. We deduce that the p-type composite with low graphene content arises from the doping induced by alumina matrix. When the average thickness of FG flake increases, the graphene layers that do not contact with the matrix compensate the doping effect and make the carrier type turned over. We believe this FG/Al_2O_3 carrier type tunable composite is very promising for novel semiconductive materials applied in harsh environments (radiation, high temperature, corrosion, etc.)

4. Experimental Section

Synthesis of GO: GO was prepared by the modified hummers method reported elsewhere.[31] Briefly, purified natural graphite (1 g, SP-1, Bay Carbon, MI) was added to a flask and filled with H_2SO_4 (25 mL) at room temperature, followed by addition of $KMnO_4$ (3.5 g) slowly at 0 °C (ice bath). After increase of temperature to 40 °C, the mixture was stirred by magnetic stirring bar for 2h. Water (200 mL) was added into the mixture and then H_2O_2 (30 wt%, 5 mL) was added to react with excess $KMnO_4$. The as-prepared GO precipitated quickly because of the strong acid environment and the clear supernatant was decanted after a few hours. The precipitate mixture was washed with HCl solution (1M, 500 mL) by vacuum filtration for several times. Then water (200 mL) was added to the mixture and dialysis for a week to remove all the remaining metal species. More water (1L) was added to the purified mixture followed by sonication to form GO colloid. Finally, the colloid was centrifuged at 4000 rpm for 30 min to remove graphite and large GO flakes. The obtained GO colloid was very stable for several months and used to prepare all the composite samples.

Measurement of GO concentration and GO weight loss: For determining the concentration of GO colloid, firstly a 50mL vial was heated at 60 °C in vacuum for 24 h and weighted immediately. Then 40 mL GO colloid was filled into the vial and heated at 80 °C to remove most of the water. Finally the dried GO and vial were heated at 60 °C in vacuum for further desiccation and then weighted immediately. From the weight difference between the vial with dried GO and empty vial the concentration of GO colloid can be calculated and the result is 4.95×10^{-4} gmL^{-1}. The weight loss of GO at sintering temperature was measured by TGA using Rigaku Thermoplus2 thermo-gravimetric analyzer. The heating rate was 20 °C min^{-1} under 100 °C, 5 °C min^{-1} from 100 °C to 300 °C and 20 °C min^{-1} again from 300 °C to 1300 °C. The temperature was holding at 100 °C for 10 min to remove the adsorbing water. GO sample (~5 mg) was measured in a platinum crucible under argon gas flow from room temperature to 1300 °C.

Measurement of Zeta potentials: Zeta potentials of as-prepared GO colloid and α-Al_2O_3 colloid (1×10^{-3} gmL^{-1}) were measured using Zetasizer Nano ZS (Malvern, UK). This instrument utilizes Laser Doppler Micro-electrophoresis technique to measure zeta potential with a red laser (633nm). The pH values of both samples were adjusted by MPT-2 Autotitrator (Malvern, UK) using HCl and NaOH solutions (0.01M). Before measurement, both samples were sonicated for 0.5h to achieve homogeneous dispersion.

Preparation of GO/Al_2O_3 hybrids: The commercially available α-Al_2O_3 powder (TM-DAR, Taimei Chemicals Co. Ltd., Tokyo, Japan), with a purity of 99.99% and an average particle size of 0.2 μm was used in this study. As-received α-Al_2O_3 (5 g) was directly poured into a beaker without any treatment. Then water (500 mL) was added and the pH was adjusted to around 3.33 using HCl solution (1 M). After 1h sonication, an Al_2O_3 colloid was formed. Two mixing methods have been exploited to prepare powder composites. In one method, certain amount of GO colloid (70 mL, 80 mL, 90 mL, 100 mL and 110 mL) was added to the Al_2O_3 colloid by titration while stirring. In the other method, the titration process was reversed in which Al_2O_3 colloid was added to the GO colloid. The mixture was separated by vacuum filtration followed by drying at 80 °C.

Sintering of FG/Al_2O_3 composites: The bulk composites were prepared using SPS apparatus (Dr. Sinter 511-S, Sumitomo Coal Mining Co. Ltd., Japan). GO/Al_2O_3 hybrid powder was loaded into a 12 mm inner diameter graphite die. A sheet of graphitic paper was placed between the punch and the powder while BN were sprayed between the die and powder for easy removal. The powders were sintered in a vacuum (residual cell pressure <6 Pa). The soaking time was 5 min and the heating rate was 100 K min^{-1}. The pressure was applied in two steps: the initial pressure of 32 MPa was applied, and consequently the pressure was increased to 60 MPa from 1000 °C upwards and maintained during the dwelling time at 1300 °C.

Calculation of filler volume fraction in composites: The mass loss of GO in composites during sintering was estimated by measuring the mass loss of GO without Al_2O_3. Certain amount of dried GO was loaded into

the graphite die without applied uniaxial pressure. GO was experienced the same procedure in sintering of FG/Al_2O_3 composites by using SPS apparatus. After cooling the heated GO was taken out and its weight was measured. It was calculated that 35% mass remained after sintering procedure. The calculated mass loss percentage was used to estimate the filler volume fraction in composites. The density of FG (2.28 gcm^{-1}) and α-Al_2O_3 (3.96 gcm^{-1}) were used to calculate the filler volume fraction in composites.

Characterization: The morphology and microstructure of samples were characterized by field emission SEM (JEOL JSM-6700F), TEM and HRTEM (JEOL 200CX). XPS measurements were performed with PHI5600 equipment (Ulvac Phi, Kanagawa, Japan); for testing the graphene after sintering, the composite prepared from the GO/Al_2O_3 hybrid with GO content of 0.79wt.% was used. Micro-Raman measurements were made with a SOLAR TII Nanofinder (Tokyo Instruments Co.) with 532 nm wavelength incident laser light and a 100× objective. The electrical conductivity and Hall coefficient were measured by Van der pauw method by using a Hall mearsurement system (ResiTest 8300 series, Toyo Corp., Japan).

Supporting Information

Supporting Information is available from the Wiley Online Library or from the author.

Acknowledgements

This work is funded by Natural Science Foundation of China (No.51074054). We would like to thank Prof. Hitoshi Takamura, Prof. Fumio Saito, Prof. Rong Tu, Dr. Qiwu Zhang and Mr. Hideyuki Magara in Tohoku University for their generous help.

Received: March 6, 2012
Revised: April 10, 2012
Published online: May 29, 2012

[1] X. Y. Yang, X. Y. Zhang, Y. F. Ma, Y. Huang, Y. S. Wang, Y. S. Chen, *J. Mater. Chem.* **2009**, *19*, 2710.
[2] a) D. H. Wang, D. W. Choi, J. Li, Z. G. Yang, Z. M. Nie, R. Kou, D. H. Hu, C. M. Wang, L. V. Saraf, J. G. Zhang, I. A. Aksay, J. Liu, *ACS Nano* **2009**, *3*, 907; b) D. H. Wang, R. Kou, D. Choi, Z. G. Yang, Z. M. Nie, J. Li, L. V. Saraf, D. H. Hu, J. G. Zhang, G. L. Graff, J. Liu, M. A. Pope, I. A. Aksay, *ACS Nano* **2010**, *4*, 1587.
[3] a) S. Chen, J. W. Zhu, X. D. Wu, Q. F. Han, X. Wang, *ACS Nano* **2010**, *4*, 2822; b) F. H. Li, J. F. Song, H. F. Yang, S. Y. Gan, Q. X. Zhang, D. X. Han, A. Ivaska, L. Niu, *Nanotechnology* **2009**, *20*, 455602; c) S. Watcharotone, D. A. Dikin, S. Stankovich, R. Piner, I. Jung, G. H. B. Dommett, G. Evmenenko, S. E. Wu, S. F. Chen, C. P. Liu, S. T. Nguyen, R. S. Ruoff, *Nano Lett.* **2007**, *7*, 1888.
[4] H. Bai, C. Li, G. Q. Shi, *Adv. Mater.* **2011**, *23*, 1089.
[5] S. B. Yang, X. L. Feng, S. Ivanovici, K. Mullen, *Angew. Chem.-Int. Edit.* **2010**, *49*, 8408.
[6] C. Z. Zhu, S. J. Guo, P. Wang, L. Xing, Y. X. Fang, Y. M. Zhai, S. J. Dong, *Chem. Commun.* **2010**, *46*, 7148.
[7] Y. C. Fan, L. J. Wang, J. L. Li, J. Q. Li, S. K. Sun, F. Chen, L. D. Chen, W. Jiang, *Carbon* **2010**, *48*, 1743.
[8] C. N. R. Rao, A. K. Sood, K. S. Subrahmanyam, A. Govindaraj, *Angew. Chem.-Int. Edit.* **2009**, *48*, 7752.
[9] L. S. Walker, V. R. Marotto, M. A. Rafiee, N. Koratkar, E. L. Corral, *ACS Nano* **2011**, *5*, 3182.
[10] M. Kosmulski, *Colloid Surf. A-Physicochem. Eng. Asp.* **1995**, *95*, 81.
[11] D. R. Dreyer, S. Park, C. W. Bielawski, R. S. Ruoff, *Chem. Soc. Rev.* **2010**, *39*, 228.
[12] a) M. Kosmulski, *J. Colloid Interface Sci.* **2006**, *298*, 730; b) M. Kosmulski, *J. Colloid Interface Sci.* **2009**, *337*, 439; c) M. Kosmulski, *J. Colloid Interface Sci.* **2011**, *353*, 1.
[13] D. H. Everett, *Basic Principles of Colloid Science*, The Royal Society of Chemistry, London **1988**.
[14] M. Estili, A. Kawasaki, H. Sakamoto, Y. Mekuchi, M. Kuno, T. Tsukada, *Acta Mater.* **2008**, *56*, 4070.
[15] H. A. Becerril, J. Mao, Z. Liu, R. M. Stoltenberg, Z. Bao, Y. Chen, *ACS Nano* **2008**, *2*, 463.
[16] I. Jung, D. A. Field, N. J. Clark, Y. W. Zhu, D. X. Yang, R. D. Piner, S. Stankovich, D. A. Dikin, H. Geisler, C. A. Ventrice, R. S. Ruoff, *J. Phys. Chem. C* **2009**, *113*, 18480.
[17] a) S. Stankovich, D. A. Dikin, R. D. Piner, K. A. Kohlhaas, A. Kleinhammes, Y. Jia, Y. Wu, S. T. Nguyen, R. S. Ruoff, *Carbon* **2007**, *45*, 1558; b) L. Liu, S. M. Ryu, M. R. Tomasik, E. Stolyarova, N. Jung, M. S. Hybertsen, M. L. Steigerwald, L. E. Brus, G. W. Flynn, *Nano Lett.* **2008**, *8*, 1965.
[18] M. M. Lucchese, F. Stavale, E. H. M. Ferreira, C. Vilani, M. V. O. Moutinho, R. B. Capaz, C. A. Achete, A. Jorio, *Carbon* **2010**, *48*, 1592.
[19] A. C. Ferrari, J. Robertson, *Phys. Rev. B* **2000**, *61*, 14095.
[20] L. M. Malard, M. A. Pimenta, G. Dresselhaus, M. S. Dresselhaus, *Phys. Rep.-Rev. Sec. Phys. Lett.* **2009**, *473*, 51.
[21] a) D. Zhan, Z. H. Ni, W. Chen, L. Sun, Z. Q. Luo, L. F. Lai, T. Yu, A. T. S. Wee, Z. X. Shen, *Carbon* **2011**, *49*, 1362; b) A. Ganguly, S. Sharma, P. Papakonstantinou, J. Hamilton, *J. Phys. Chem. C* **2011**, *115*, 17009.
[22] E. J. Garboczi, K. A. Snyder, J. F. Douglas, M. F. Thorpe, *Phys. Rev. E* **1995**, *52*, 819.
[23] S. Rul, F. Lefevre-schlick, E. Capria, C. Laurent, A. Peigney, *Acta Mater.* **2004**, *52*, 1061.
[24] G. D. Zhan, J. D. Kuntz, J. E. Garay, A. K. Mukherjee, *Appl. Phys. Lett.* **2003**, *83*, 1228.
[25] J. H. Chen, C. Jang, S. D. Xiao, M. Ishigami, M. S. Fuhrer, *Nat. Nanotechnol.* **2008**, *3*, 206.
[26] G. Eda, G. Fanchini, M. Chhowalla, *Nat. Nanotechnol.* **2008**, *3*, 270.
[27] Y. Y. Wang, Z. H. Ni, T. Yu, Z. X. Shen, H. M. Wang, Y. H. Wu, W. Chen, A. T. S. Wee, *J. Phys. Chem. C* **2008**, *112*, 10637.
[28] F. Varchon, R. Feng, J. Hass, X. Li, B. N. Nguyen, C. Naud, P. Mallet, J. Y. Veuillen, C. Berger, E. H. Conrad, L. Magaud, *Phys. Rev. Lett.* **2007**, *99*, 126805.
[29] N. Mounet, N. Marzari, *Phys. Rev. B* **2005**, *71*, 205214.
[30] M. K. Loudjani, C. Haut, *J. European Ceram. Soc.* **1996**, *16*, 1099.
[31] S. Park, J. H. An, R. D. Piner, I. Jung, D. X. Yang, A. Velamakanni, S. T. Nguyen, R. S. Ruoff, *Chem. Mat.* **2008**, *20*, 6592.